23rd ABCM International Congress of Mechanical Engineering
December 6-11, 2015, Rio de Janeiro, RJ, Brazil

A DIRECTIONAL IMMERSED BOUNDARY METHOD FOR FLOW PAST SOLID OBSTACLES

João Rodrigo Andrade
Aristeu da Silveira-Neto
João Marcelo Vedovoto
Federal University of Uberlândia - Campus Santa Mônica - 5P Block - Avenue João Naves de Ávila - 2121 - Santa Mônica neighborhood- Uberlândia - MG - CEP 38400-902
jandrade@mec.ufu.br, aristeus@mecanica.ufu.br, jmvedovoto@mecanica.ufu.br

Abstract. *In present work it is proposed a variation of the Multi-Direct Forcing Method, a discrete and iterative forcing approach of the immersed boundary methods. The proposed modification was introduced in the body force interpolation and distribution functions between the Eulerian and Lagrangian grids. which the body force is only evaluated and spread in the discrete volumes surrounding Cartesian grids in the fluid side, instead of both fluid and solid sides. To verify the CFD code, ensure that it has been coded correctly and check its convergence order, the Method of Manufactured Solutions was used. To validate and compare the new method, both the original Multi-Direct Forcing Method and the proposed modified method, were applied three different simulation cases: a two-dimensional laminar flow past a circular cylinder, a three-dimensional laminar flow past a sphere and a large eddy simulation (LES) of a turbulent flow around an airfoil. The whole equations are demonstrated and the improvement and the limitations of the new strategy is discussed.*

Keywords: *Immersed-Boundary method, indirect iterative boundary condition imposition, body force interpolation function, directional forcing distribution*

1. INTRODUCTION

The Immersed Boundary Method(IBM) was first proposed by Peskin (1977) to simulate blood flow in heart valves, a high complex problem that involves moving boundaries and complex geometries. The central idea of the Peskin method is the use of two independent meshes, an Eulerian mesh which is used to calculate the fluid flow equations and an independent Lagrangian mesh representing the immersed body. The communication between both meshes is made through a force source term added to the momentum equation.

Since Peskin created this approach, many others researchers have been using the IBM successfully in various applications. Their applications cover a broad spectrum of fluid dynamics problems from flow through heart devices (Peskin 1972, Peskin 1977), to the interaction of body movement and fluid flow (Mittal, 2005), modeling anguilliform swimming (Tyson, 2008) and 3-D parachute simulation (Kim, 2009). Reviews of IB methods may be found in Mittal (2005) and Margnat (2009). Two classes of methods are discussed depending on how the source terms describing the presence of the boundary are imposed: directly in the continuous equations describing the flow (continuous forcing approach) or in the resulting system of linear equations (discrete forcing approach).

Several different immersed boundary methods can be found in the literature. They can be classified as either diffuse (continuous) methods or sharp (discrete) methods (Marella 2005, Martin 1996, Berthelsen 2008). The diffuse methods are considered to be considered no straightforward how the boundary conditions should be imposed at the immersed boundary. The boundary conditions are enforced through a smoothed forcing term added to the momentum equation (Berthelsen, 2008). One disadvantage with the diffuse methods is that the effect of the boundary is distributed over a band of several grid points which smear out discontinuities across the boundary. This smearing has an unfavorable effect on the accuracy of the numerical scheme (Berthelsen, 2008).

In present work it is used a diffuse directional distribution (herein, refer to as the *directional IBM*) forcing strategy which spreads the body force just outside the immersed boundary, the source term which represents the body force is derived from momentum equation by setting the velocity at the boundary (Lagrangian IB points) to the desired and known velocity field applying directional interpolation/distribution delta functions. In latest work, similar forcing strategy was applied by Zhang (2007) in simulating laminar flows, A. Cristallo (2006) in simulating turbulent flows together with the LES and a simple WLM and Ji (2012) with a turbulent flow around a cylinder. Good agreement was achieved when comparing numerical results with published experimental data. Second-order spacial accuracy of this strategy has been reported by Zhang (2007), although only a linear delta function was used. In present work, it was applied both the *directional IBM* and the original *Multi-direct forcing* (herein, refer to as the *MDF*) strategies for the purpose of giving a comparative view on their influences on the accuracy of numerical results (Ji, 2012).

First, to verify the in-house computational algorithm, the Method of Manufactured Solutions (Vedovoto, 2011) is applied so that the Lagragian and Eulerian domains are fully verified. Than, preliminary numerical results of three distinct test cases which are simulated and compared to literature is presented, they are: a two-dimensional flow past a stationary circular cylinder at Reynolds number $Re = 40$ and $Re = 100$, a three-dimensional flow past a stationary sphere at Reynolds number $Re = 100$ and finally a two-dimensional flow past a stationary airfoil at a range of angles of attack ranging from 0^o to 15^o, the airfoil profile is a NACA0012 (National Advisory Committee for Aeronautics). The turbulence modeling methodology used was the Large Eddy Simulation (LES) with the dynamic Smagorinsky algebraic sub-grid scale model (Germano et al., 1991) to calculate the turbulent viscosity. A fully implicit scheme is adopted for all cases calculated. The central difference scheme (CDS) is applied to express both the diffusive and advective contributions of the transport equations. Since the developed numerical code adopts a pressure-velocity coupling based on pressure variations, an appropriate algorithm for pressure-velocity coupling is needed.

2. METHODOLOGY

2.1 Mathematical Modeling

2.1.1 Mathematical Model for Fluid Domain

A rectangular domain was used for the present simulations and it was discretized with an Eulerian grid. The filtered Navier-Stokes equations for a viscous incompressible fluid can be written as Eq. 1.

$$\rho\left[\frac{\partial u_i}{\partial t}+\frac{\partial (u_i u_j)}{\partial x_j}\right] = -\frac{\partial p}{\partial x_i}+\frac{\partial}{\partial x_j}\left[(\nu+\nu_t)\left(\frac{\partial u_i}{\partial x_j}+\frac{\partial u_j}{\partial x_i}\right)\right]+f_i, \tag{1}$$

$$\frac{\partial u_i}{\partial x_i}=0, \tag{2}$$

Concerning turbulence modeling, Eq.1 is already shown as a filtered equation in a LES Framework, Eq. 2 is the continuity equation for incompressible flow. The Boussinesq hypothesis was used to model the subgrid Reynolds stress tensor.

2.2 Immersed Boundary Method

In this Section, some mathematical and computational information relevant to the used immersed boundary methods are presented.

2.2.1 Interpolation and distribution strategies

To model the communication between Eulerian and Lagrangian meshes, it is introduced two functions $I(\phi)$ and $D(\Phi)$ which represent the interpolation and distribution functions, respectively. For convenience the lower-case ϕ represents the variables on the fluid domain $\vec{x}$ (Cartesian grid, Eulerian domain), e.g. u, p, f, and the upper-case Φ indicates the variables on the IB points $\vec{X}_k$ (Lagrangian domain), such as U_k, F.

The original interpolation and distribution interaction function between the immersed boundary and the fluid are given by Eqs. 3 and 4, respectively.

$$\vec{\Phi}(\vec{X}_k,t) = I\left(\vec{\phi},\vec{X}_k,t\right) = \sum_{\vec{x}\in\Omega}\vec{\phi}(\vec{x},t)\delta_h(\vec{x}-\vec{X}_k)\Delta V_i, \tag{3}$$

$$\vec{\phi}(\vec{x},t) = D\left(\vec{\Phi},\vec{x},t\right) = \sum_{\Omega_{Lag}}\vec{\Phi}(\vec{X}_k,t)\delta_h(\vec{x}-\vec{X}_k)\Delta A_k\Delta S_k, \tag{4}$$

where, Ω represents the set of Cartesian grids both inside and outside the immersed boundary, Ω_{Lag} represents the Lagrangian points over the immersed boundary, ΔV_i is the volume of control volume where the Lagrangian point k lies within, $\delta_h(\vec{x}-\vec{X}_k)$ is a weight-pondered function.For the directional interpolation/distribution strategy, just a part of the volume in the boundary of the Lagrangian point is used, these functions are similar to the above except a renormalization factor N_d that is applied and the region reached by the discrete delta function. So, the variables $\vec{\Phi}(\vec{X}_k,t)$ and $\vec{\phi}(\vec{x},t)$ on the Cartesian grids only outside the immersed boundary are calculated as:

$$\vec{\Phi}(\vec{X}_k,t) = I_d\left(\vec{\phi},\vec{X}_k,t\right) = \sum_{\vec{x}\in\Omega_d}\frac{1}{N_d}\vec{\phi}(\vec{x},t)\delta_h(\vec{x}-\vec{X}_k)\Delta V_i, \tag{5}$$

$$\vec{\phi}(\vec{x},t) = D_d\left(\vec{\Phi},\vec{x},t\right) = \sum_{\Omega_{Lag}}\frac{1}{N_d}\vec{\Phi}(\vec{X}_k,t)\delta_{h_d}(\vec{x}-\vec{X}_k)\Delta A_k * \Delta S_k, \tag{6}$$

and

$$N_d = \sum_{\vec{x} \in \Omega_d} \delta_h(\vec{x} - \vec{X}_k), \tag{7}$$

here, Ω_d represents the set of Cartesian grids only in the fluid domain, outside the immersed boundary, δ_{h_d} represents the outside portion of the discrete dirac function. The difference between both distribution/interpolation strategies is better illustrated in Fig. 1.

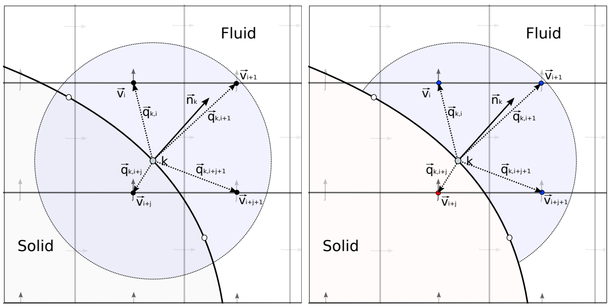

(a) (b)

Figure 1. Difference between delta function scheme. Schematic diagram for the interpolation strategy: (a) Original delta function; (b) directional delta function

These interpolation/distribution equations are applied for velocity and body forces and solved on the Eulerian/Lagrangian meshes, hence the Eqs. 5 and 6 become:

$$\vec{U}(\vec{X}_k, t) = I_d\left(\vec{u}, \vec{X}_k, t\right) = \sum_{\vec{x} \in \Omega_d} \frac{1}{N_d} \vec{u}(\vec{x}, t) \delta_h(\vec{x} - \vec{X}_k) \Delta V_i, \tag{8}$$

$$\vec{f}(\vec{x}, t) = D_d\left(\vec{F}, \vec{x}, t\right) = \sum_{\Omega_{Lag}} \frac{1}{N_d} \vec{F}(\vec{X}_k, t) \delta_{h_d}(\vec{x} - \vec{X}_k) \Delta A_k \Delta S_k, \tag{9}$$

2.2.2 Computational Algorithm

First, an estimate of the velocity can be obtained by Eq. 10. Note that the Euler time discretization scheme is used here for the sake of simplicity. The subscript p stands for the inner loop of the IBM and start evaluated as $p = 1$.

$$\vec{u}_p^*(\vec{x}_k, t) = \vec{u}(\vec{x}_k, t)^n + \Delta t \left[r\vec{h}s\right]^n, \tag{10}$$

Next, the intermediate velocity at grid points is obtained and the force terms at Lagrangian points are calculated.

$$\vec{F}_p(\vec{x}, t) = \frac{\vec{U}(\vec{X}_k, t) - \vec{U}_p^*(\vec{X}_k, t)}{\Delta t}. \tag{11}$$

The Lagrangian forces are distributed among the Eulerian points and, finally, the intermediate velocities are corrected.

$$\vec{u}_{p+1}^*(\vec{x}_k, t) = \vec{u}_p^*(\vec{x}_k, t) + \vec{f}_p \cdot \Delta t. \tag{12}$$

If the convergence is not achieved then go back to Eq. 10.

3. VERIFICATION AND VALIDATION STUDIES

3.1 Application of the method of manufactured solutions to the verification of the immersed boundary implementation

These manufactured solutions modify the original equations by adding a 'source term', such as those presented in transport equations (Vedovoto, 2011). For the verification of the implemented methods, Vedovoto (2011) proposes analytic solution (Eq. 13-16).

$$u_e = sin^2\left(\alpha_s \pi x + \beta_s \pi y + \gamma_s \pi z + \delta_s t\right), \tag{13}$$

$$v_e = -cos^2\left(\alpha_s \pi x + \beta_s \pi y + \gamma_s \pi z + \delta_s t\right), \tag{14}$$

$$w_e = \frac{\alpha_s}{\gamma_s} cos^2\left(\alpha_s \pi x + \beta_s \pi y + \gamma_s \pi z + \delta_s t\right) + \frac{\beta_s}{\gamma_s} cos^2\left(\alpha_s \pi x + \beta_s \pi y + \gamma_s \pi z + \delta_s t\right), \tag{15}$$

$$p_e = cos\left(\alpha_s \pi x + \beta_s \pi y + \gamma_s \pi z + \delta_s t\right), \tag{16}$$

The subscript e stands for the manufactured solutions of the primary variables, i.e. the three velocity components and pressure; t is the time. It is observed that, if the divergence of Eqs. (13)-(16) is taken, the incompressibility condition is verified (Vedovoto, 2011).

The computational domain considered for the present numerical simulations is a cube of dimensions $[0,1][0,1][0,1]$, in x, y and z directions respectively. The time step is controlled taken the CFL factor smaller than 0.25. The parameters α_s, β_s and γ_s are set to 2, and $\delta_s = 1$. The constant values of density and viscosity are set to unity and 0.01, respectively.

A sphere of radius $0.25\ m$, discretized by a surface of triangles, is placed at the position $x = y = z = 0.5\ m$. The procedure used for evaluating the error rate of decay is the same presented in Vedovoto et *al*. (2011), for the evaluation of the global convergence rate of the numerical scheme. From an Eulerian grid of 128^3, the Eulerian grid is halved three times, resulting 4 different grid sizes.

The rate of convergence is estimated using the L_2 norm (Vedovoto et al., 2011). The in-house code developed have shown second order of convergence rate for velocity as well as for the immersed boundary.

3.2 Laminar flow past 2D stationary circular cylinder

A laminar flow past a two-dimensional stationary circular cylinder, one of the benchmark problems, is calculated to verify the method developed in this work. This case has been investigated experimentally and numerically for many years. In this study, a domain with $W/D = 35$, $L/D = 50$ was adopted, where L is the domain horizontal length, W is the vertical length and D is the cylinder diameter. For our simulations at Reynolds number $Re = 40$ an $Re = 100$, a computational mesh of 714.100 volumes was used. The time step size was determined to make the maximum CFL number approximately equal to 0.25. A Dirichlet boundary condition $(u/u_\infty = 1; v = 0)$ is used at the inflow and farfield boundaries, the Dirichlet boundary is also used at cylinder surface $u = 0, v = 0$ and a Robin-type boundary condition is adopted at the outflow.

Figure 2 shows comparisons between the original MDF and the present method (directional IBM) of the streamlines neighbouring the cylinder for Reynolds number equal to 40 after the flow had reached a steady after symmetric state. The length of the recirculation zone, the location of the vortex centers and the angle of separation are given in Tab. 1, where they are compared with experimental and other numerical results. This indicates that the boundary condition is satisfied. Figure 3 illustrates the iso-vorticity contours for $Re = 40 - 100$. Comparison is made among the directional IBM, the

Table 1. Steady uniform flow past a circular cylinder for $Re = 40$: length L of recirculation zone, location (a, b) of vortex centre and separation angle θ (nomenclature given in Fig. 3).

	L/D	a/D	b/D	θ
Coutanceau (1977)	2.13	0.76	0.59	53.5
Linnick (2005)	2.28	0.72	0.60	53.6
Herfjord (1996)	2.25	0.71	0.60	51.2
Original MDF	2.25	0.75	0.60	54.0
Present study	2.28	0.77	0.60	53.0

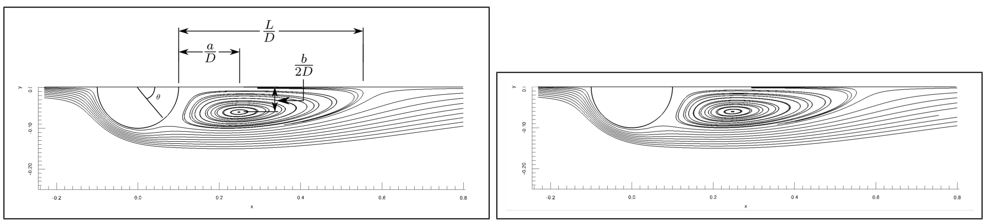

(a) (b)

Figure 2. The streamlines for $Re = 40$ and nomenclature used in Tab. 1. (c) original MDF; (e) directional IBM.

original MDF and the literature results reported by Jungwoo Kim (2001). The good agreement is evident. The flow is symmetric about the streamwise axis at $Re = 40$, whereas vortex shedding takes place at $Re = 100$, indicating that the vorticity field is well captured by the present immersed-boundary method.

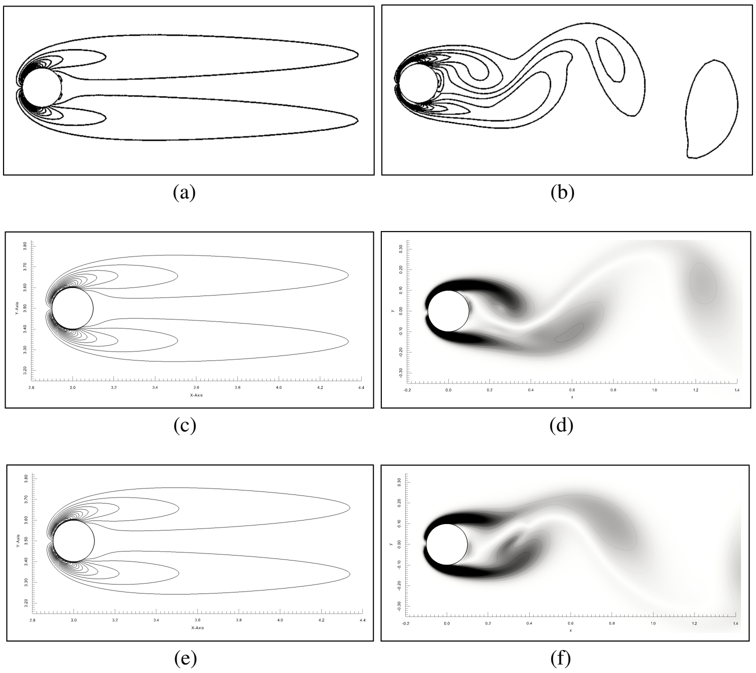

Figure 3. Iso-vorticity contours near a circular cylinder for $Re = 40$: (a) Jungwoo Kim (2001); (c) original MDF; (e) directional IBM. For $Re = 100$: (b) Jungwoo Kim (2001); (d) original MDF; (f) directional IBM. Instantaneous vorticity contours are drawn.

3.3 Flow past a sphere

A laminar flow past a three-dimensional stationary sphere, another well known benchmark problems, is calculated to verify the method developed in this work in a three dimensional case. A domain with dimensions $[25D, 10D, 10D]$ was adopted, in direction x, y and z, respectively, where D is the sphere diameter. For our simulations at Reynolds number $Re = 100$, a computational mesh of 4.224.100 volumes was used. The time step size was determined to make the maximum CFL number approximately equal to 0.25. On the surface of the sphere, the no-slip condition is applied, Dirichlet boundary condition $(u/u_\infty = 1; v = 0; w = 0)$ is used at the inflow and farfield boundaries, and a Robin-type boundary condition is adopted at the outflow.

Streamlines for this regime are shown in Fig. 4, which shows the (x, y)-planes for Reynolds number 100. The flow is seen to separate from the surface of the sphere at an angle θ and rejoin to form a closed separation bubble and a toroidal vortex, where the velocity is zero in the sphere's reference frame. The numerical results of Johnson (1999) provides data for comparison with the present results. Good agreement between the current results is shown. Figure 5 shows

Table 2. Steady uniform flow past a sphere for $Re = 100$.

	$x_c(m)$	$y_c(m)$	x_S(m)	$\theta_S(o)$
Johnson (1999)	0.72	0.26	1.23	126
Original MDF	0.77	0.25	1.29	125
Present study	0.80	0.28	1.33	128

an oblique view of the iso-vorticity contour for each of the two methods tested. These oblique views help convey the three-dimensional form of the stationary structures. They seen to be almost similar, showing that the new method does not lose quality and accuracy at this Reynolds number ($Re = 100$).

3.4 Flow past a airfoil NACA 0012

In the numerical structure of IB method, the pressure is solved both inside and outside the immersed boundary as a whole. A drawback about the use of the MDF in this kind of problem is that the pressure coupling between inside

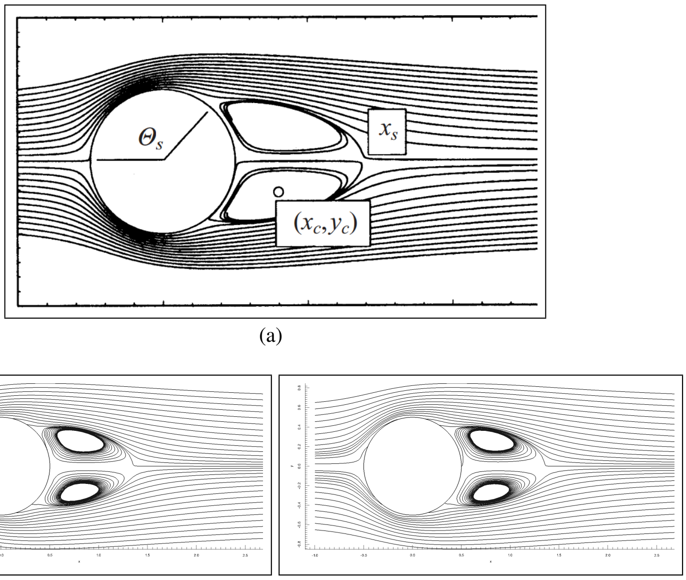

(a)

(b) (c)

Figure 4. Computed axisymmetric streamlines past the sphere: (a)Johnson (1999) ; (b)original MDF; (c)directional IBM.

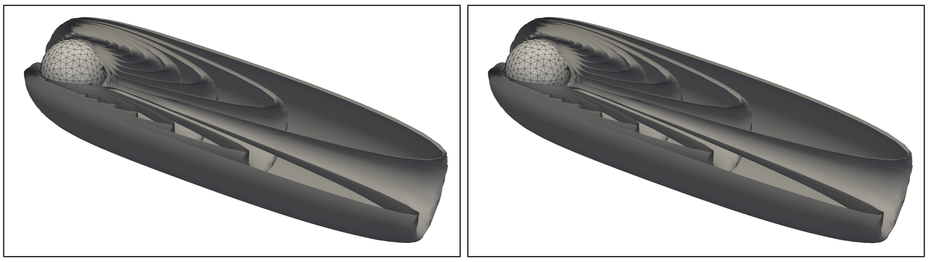

(a) (b)

Figure 5. Oblique views of the stationary vortical structure:(a) original MDF; (b) directional IBM.

and outside may lead to spurious results when the immersed body is thin, according to Ji (2012). Then, as the method developed herein is objectified to improve the solution in highly irregular boundaries, to really gauge the generality of the proposed method, a simulation of flow past an airfoil was carried out. Figure 6 illustrate the difference between the original and the directional distribution/interpolation functions on an airfoil trailing edge mesh. The simulations were

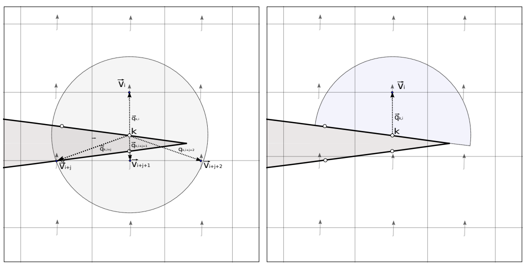

(a) (b)

Figure 6. Schematic diagram for the interpolation scheme on an airfoil trailing edge mesh: (a) Original delta function and (b) Directional delta function

carried out on a two-dimensional grid, the calculation domain has a length of $9C$ and a width of $5C$, where C is the airfoil chord. A non-uniform cartesian grid of 522.000 volume with three distinct refined regions in each direction was used.

The airfoil is placed at $3.3C$ from the left boundary and centered vertically at $2.5C$. A constant velocity profile was imposed at the domain inlet, in such a way that the fluid goes from the left to the right boundary. Neumann condition was imposed for the velocity at all other faces, on the surface of the airfoil, the no-slip condition is applied. The time step is controlled taken the CFL factor smaller than 0.25. The dynamic Smagorinsky turbulence model (to perform LES) was employed to simulate two cases at $Re = 10^4$ and $Re = 10^5$. Results reported by Akbari and Price (2003) predicted the static stall angle at $\alpha \approx 15^o$ for Reynolds numbers of 10^4. Figure 7 shows the lift (C_l) coefficients versus the angle-of-attack for both test case. The simulations were carried out for $100s$ physical. It can be seen that neither the original MDF nor the directional IBM a good agreement has been achieved. Figure 8 shows the iso-vorticity contours near the airfoil for both method calculated. It can be seen that the vortical flow structures are decoupled inside and outside the immersed boundary by the body force. In the original MDF, the grids within the body is more affected by the flow outside outside than the directional IBM, due to the linear discrete delta function used in this case. Because the directional IBM forcing strategy only distributes the body force to the grids outside the immersed boundary, this influence confines the flow within the immersed boundary. On the other hand, also due to the delta function used in directional IBM, non-physical recirculation appears on the bottom of the airfoil.

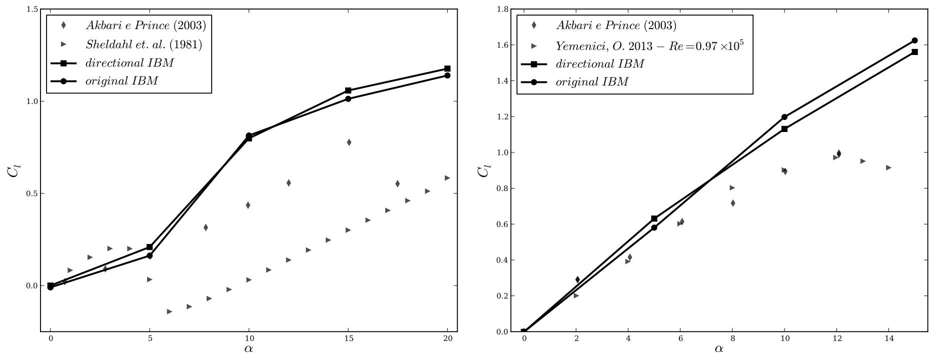

(a) (b)

Figure 7. Lift coefficient comparison between experimental and numerical data at Reynolds (a) $Re = 10^4$; (b) $Re = 10^5$.

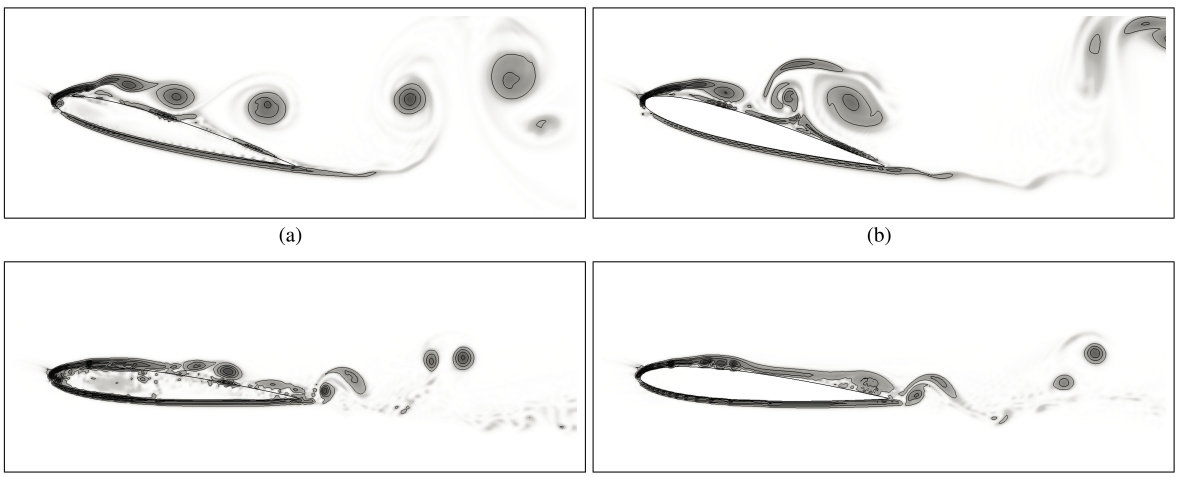

(a) (b)

(c) (d)

Figure 8. Iso-vorticity contours near the airfoil NACA 0012 for $Re = 10^4$ and $Re = 10^5$: (a) original MDF at $Re = 10^4$; (b) directional IBM at $Re = 10^4$; (c) original MDF at $Re = 10^5$; (d) directional IBM at $Re = 10^5$;. Instantaneous vorticity contours are drawn.

4. RESULTS AND DISCUSSIONS

The results of the iterative IB method using the directional strategy show an improvement but are still not that close to those using body-conformal grids simulating highly sharp boundaries. However, both original MDF and directional IBM predicted very well the flow past the cylinder and the sphere. More accurate schemes can be found among the category of sharp methods. In these methods the numerical discretization near the immersed boundary is modified so that the boundary conditions are imposed directly at the location of the boundary Ji (2012). So we can state that even if the direction of interpolation and distribution is appropriate for sharp geometries, diffuses methods can not have high accuracy with a smooth solution neighboring the solid immersed.

5. ACKNOWLEDGEMENTS

The authors acknowledge CNPQ, CAPES, PROEX, PROPP, FAPEMIG and PETROBRAS for the financial support and the School of Mechanical Engineering of the Federal University of Uberlândia for the technical support.

6. RESPONSIBILITY NOTICE

The authors are the only responsible for the printed material included in this paper.

7. REFERENCES

A. Cristallo, R.V., 2006. "Combined immersed boundary/large-eddy-simulations of incompressible three dimensional complex flows." *Flows, Turbulence and Combustion 77*, Vol. 77, 3-26.

Berthelsen, P. A.; Faltinsen, O.M., 2008. "A local directional ghost cell approach for incompressible viscous flow problems with irregular boundaries." *Journal of Computational Physics*, Vol. 227, 4354-4397.

Coutanceau, M. Bouard, R., 1977. "Experimental determination of the main features of the viscous flow in the wake of a circular cylinder in uniform translation part 1. steady flow." *J. Fluid Mech.*, Vol. 79:231-256.

Herfjord, K., 1996. "A study of two-dimensional separated flow by a combination of the finite element method and navier-stokes equations." *Dr. Ing.-Thesis, Norwegian Institute of Technology, Department of Marine Hydrodynamics, Trondheim, Norway*.

Ji, C.; Munjiza, A.W.J., 2012. "A novel iterative direct-forcing immersed boundary method and its finite volume applications". *Journal of Computational Physics*, Vol. 231:1797-1821.

Johnson, T. A. Patel, V.C., 1999. "Flow past a sphere up to a reynolds number of 300." *Journal of Fluid Mechanics*, Vol. 378, 19-70.

Jungwoo Kim, ; Dongjoo Kim, a.H.C., 2001. "An immersed-boundary finite-volume method for simulations of flow in complex geometries." *Journal of Computational Physics*, Vol. 171,132-150.

Kim, Y.P.C.S., 2009. "3-d parachute simulation by the immersed boundary method." *Computational Fluids*, Vol. 38:1080-90.

Linnick, M. N. Fasel, H., 2005. "A high-order immersed interface method for simulating unsteady compressible flows on irregular domains." *J. Comput. Phys.*, Vol. 204:157-192.

Marella, S.;Krishnan, S.L.H.H., 2005. "Sharp interface cartesian grid method i: an easily implemented technique for 3d moving boundary computations." *Journal of Computational Physics*, Vol. 210, 1-31.

Margnat, F.; MoriniÃÍre, V., 2009. "Behaviour of an immersed boundary method in unsteady flows over sharp-edged bodies." *Computational Fluids*, Vol. 38:1065-79.

Martin, D.F.;Cartwright, K., 1996. "Solving poisson's equation using adaptive mesh refinement." *Technical Report UCB/ERI M96/66, U.C. Berkeley, California, USA*.

Mittal, R. Iaccarino, G., 2005. "Immersed boundary methods". *Annual Reviews of Fluid Mechanics*, Vol. 37, 239-261.

Peskin, C., 1972. "Flow patterns around heart valves: A numerical method." *Jounal of Computational Physics*, Vol. 10, 252-271.

Peskin, C., 1977. "Numerical analysis of blood flow in the heart." *Jounal of Computational Physics*, Vol. 25:220-52.

Tyson, R. Jordan, C.E.H.J., 2008. "Modelling anguilliform swimming at intermediate reynolds number: a review and a novel extension of immersed boundary method applications." *Computational Methods for Applied Mechanical Engineering*, Vol. 197:2105-18.

Vedovoto, J.M., 2011. *Mathematical and numerical modeling of turbulent reactive flows using a hybrid LES / PDF methodology.* Ph.D. thesis.

Zhang, N. Zheng, Z., 2007. "An improved direct-forcing immersed-boundary method for finite difference applications." *Journal of Computational Physics.*, Vol. New York, v. 221, p. 250-268.